A reliable sensing platform for plasmonic ELISA based on automatic flow-based methodology

Natcha Kaewwonglom[a], Miquel Oliver[b], David J. Cocovi Solberg[b,c], Katharina Zirngibl[d], Dietmar Knopp[d], Jaroon Jakmunee[a], Manuel Miró[1b]

[a]*Research Center on Chemistry for Development of Health Promoting Products from Northern Resources, Department of Chemistry, Faculty of Science, Chiang Mai University, Chiang Mai 50200, Thailand.*

[b]*FI-TRACE Group, Department of Chemistry, Faculty of Sciences, University of the Balearic Islands, E-07122 Palma de Mallorca, Illes Balears, Spain.*

[c]*University of Natural Resources and Life Sciences (BOKU), Muthgasse 18, 1190 Vienna, Austria.*

[d]*Institute of Hydrochemistry and Chemical Balneology, Chair of Analytical Chemistry and Water Chemistry, Technische Universität München, Marchioninistrasse 17, 81377 München, Germany.*

Abstract

Plasmonic enzyme-linked immunosorbent assays (ELISA) using the localized surface plasmon resonance (LSPR) of metal nanoparticles has emerged as an appealing alternative to conventional ELISA counterparts for ultrasensitive naked-eye detection of biomolecules and small contaminants. However, batchwise plasmonic ELISA involving end-point detection lacks ruggedness inasmuch as the generation or etching of NP is greatly dependent on every experimental parameter of the analytical workflow.

To tackle the above shortcomings, this paper reports on an automatic flow methodology as a reliable detection scheme of hydrogen peroxide related enzymatic bioassays for ultrasensitive detection of small molecules. Here, a competitive ELISA is combined with the in-line generation of plasmonic gold nanoparticles (AuNPs) followed by the real-time monitoring of the NP nucleation and growth rates and size distribution using a USB miniaturized photometer. Glucose oxidase was labeled to the secondary antibody and yielded hydrogen peroxide that acted as the measurand and the reducing agent of the Au(III)/citrate system in the flow network. High-throughput plasmonic assays were feasible by assembling a hybrid flow system composed of two microsyringe pumps, a perfluoroalkoxy alkane reaction coil and a 26-port multiposition valve, and operated under computer-controllable flow conditions. The ultratrace determination of diclofenac in high matrix samples, e.g., seawater, without any

*Corresponding author. E-mail: manuel.miro@uib.es

prior sample treatment was selected as a proof-of-concept application of the flow-based platform for determination of emerging contaminants via plasmonic ELISA. The detection limit (0.001 μg L^{-1}) was one order of magnitude below than that endorsed by the first EU Watch List for diclofenac as a potentially emerging contaminant in seawater, and also than that of a conventional colorimetric ELISA, which in turn resulted inappropriate for determination of diclofenac in seawater at the levels endorsed by the EU regulation. The proposed automatic fluidic approach is characterized by the reproducible timing in AuNPs nucleation and growth along with the unsupervised LSPR absorbance detection of AuNPs with a dynamic range for diclofenac spanning from 0.01 – 10 μg L^{-1}. Repeatability and intermediate precision (given as normalized signal readouts) values in seawater were < 4 % and < 14%, respectively, as compared to RSDs as high as 30% as obtained with the batchwise plasmonic ELISA counterpart.

Enzyme-linked immunosorbent assays (ELISA) adapted to different formats, e.g., direct, indirect, sandwich, and competitive ELISA are routine biochemical assays involving antigen-antibody binding for high-throughput and ultrasensitive detection of low and high molecular mass compounds in a variety of research fields including clinical,[1] environmental[2,3] and food analysis.[4] In fact, recent trends geared toward the development of ELISA tests for emerging organic pollutants, e.g., pharmaceuticals, personal care products and endocrine-disrupting chemicals, in environmental waters.[5,6] The standard ELISA protocol involves the colorimetric detection of the biochemical product of the prior enzymatic reaction; e.g., hydrogen peroxide, by resorting to organic chromophores, such as 3,3',5,5'-tetramethylbenzidine (TMB), o-phenylenediamine (OPD) and 2,2'-azino-bis(3-ethylbenzthiazoline-6-sulfonic acid) (ABTS).[1,2,4-7] However, colorimetric competitive and sandwich ELISA sensing platforms may have limited sensitivity for determination of low-molecular mass pollutants at environmentally relevant levels because the detection is merely based on the color measurement of the resulting solution by conventional photometric analysis. Especially, this comes true for detecting pollutants in marine ecosystems that are found at low ng L^{-1} (ppt) levels. For that reason, sample treatment, e.g., sample dilution, or pre-concentration stages using solid-phase extraction are quite often indispensable to achieve the required concentration range for appropriate detectability.[8,9]

Plasmonic ELISA using the localized surface plasmon resonance (LSPR) absorption of metal nanoparticles (NP) has emerged as an appealing alternative to conventional ELISA counterparts for ultrasensitive naked-eyed detection of small molecules.[10-13] This is because of the higher molar absorptivity of plasmonic AuNPs and AgNPs as compared to organic dyes[14,15] that ameliorates the detection sensitivity of the biochemical assays, and the unique optical properties of plasmonic nanomaterials. Interest has grown in recent years towards exploiting analyte-induced shifts of the LSPR absorption bands of NPs, that is, variation of particle size distribution, shape, and composition, as analytical readouts.[5,12,14] This is demonstrated by a plethora of analytical methods combining ELISA with nanotechnology which capitalized on the aggregation, etching, nucleation or growth of metal NP.[13-19]

However, plasmonic ELISA assays based on end-point measurements lack ruggedness inasmuch as the visualized results are greatly dependent on the majority of the experimental conditions, including (i) mixing time, (ii) reaction temperature, (iii) concentration and purity of reagents, (iv) competing side reactions with redox agents, (v) order of reagent addition and, most importantly, (vi) agitation mode (also in the course of optical detection through the plate reader), thus jeopardizing the repeatability of the assays because of variable reaction

rates for nanoparticle growth and etching.[13,19,20] Efforts towards halting further reaction development via addition of ancillary chemicals, such as glutathione or thiosulphate[19-22] do not offset changes in kinetic constants. In addition, the temporal resolution of naked eye protocols or conventional plate readers[14] might be insufficient for reliable monitoring of the reaction rates and detection under well-defined NP growth/etching conditions. For example, a variation of the concentration of hydrogen peroxide from a mere 119.95 μM to 120.00 μM under given reaction conditions[19] is reported to induce AuNP nucleation and lead to profound changes of the LSPR absorption bands, yet the reliability of the analytical protocol in a batchwise mode is deemed questionable. In fact, the experimental results reported in some papers dealing with batch plasmonic ELISA have been the subject matter of open debate in scientific forums (e.g., Pubpeer posts),[23] and a potential case of unethical publishing behavior.[24]

To tackle the above shortcomings, the various generations of flow analysis and miniaturized systems thereof spanning from microfluidic to millifluidic devices[25] offer viable platforms for (i) accommodation of NP-mediated assays,[26] (ii) kinetic discrimination reactions,[26] and (iii) in-line synthesis of AuNP/AgNP[26-30] on account of the controllable laminar diffusion/dispersion and reproducible timing for NP nucleation and growth as compared to batch counterparts. In contrast to standard well-plate assays, interfering effects from bovine serum albumin, along with primary and secondary antibodies immobilized on the plates, and the polymeric material itself onto the nucleation of AuNP/AgNP are entirely circumvented by resorting to bespoke fluidic approaches for reliable localized LSPR absorbance detection.[31]

In this work, an automatic flow platform inspired by the principles of flow chemistry[32] is proposed to offset the high variability in nucleation and growth kinetics of AuNP throughout plasmonic ELISA in batch format. The mesofluidic device is able to take advantage of metallic nanoprobes for reliable optical detection following monoclonal antibody-based ELISA by in-line monitoring of the time-dependent AuNP nucleation and growth unsupervised. The determination of diclofenac in waters at realistic environmental concentrations[33,34] and below the Environmental Quality Standards (EQS) endorsed by the First Watch List of the European Union[35] to identify potential emerging contaminants, that is, 0.1 μg L^{-1} in fresh and drinking waters and 0.01 μg L^{-1} in marine waters, is herein proposed as a proof-of-concept study. The feasibility of the combination of competitive ELISA with on-line plasmonic detection of hydrogen peroxide-triggered AuNP for tackling complex samples is demonstrated by the analysis of seawater without any prior sample treatment.

EXPERIMENTAL

Detailed description of reagents, samples and synthesis of the BSA-DCF conjugates is given in the SI file.

Competitive ELISA protocols for DCF

A diagrammatic description of the competitive ELISA protocol prior to on-line plasmonic NP detection is illustrated in Fig. 1. Initially, the microtiter plate was coated overnight at 4 °C with 200 µL of 0.5 µg mL^{-1} BSA-DCF according to Huebner *et al.*[6] at a pH 9.6 (0.1 mol L^{-1} $NaHCO_3$ adjusted with dilute NaOH). Then, the plate was rinsed 3 times with 400 µL of 0.05 % Tween in PBS and blocked with 400 µL of 1 g L^{-1} BSA in PBS for 1 h at room temperature (RT). Afterwards, the plate was again washed with 400 µL of PBS-Tween thrice. The competitive ELISA was carried out by adding 100 µL of DCF standard solution within the range of 0.0001 to 100 µg L^{-1} or seawater sample, whereupon 100 µL of 400 ng mL^{-1} mAb_{DCF} in PBS was added to the plate followed by incubation for 30 min at RT under gentle mixing at 100 rpm using a plate shaker. After three washing steps with PBS-Tween, 200 µL of 1:1000 diluted Ab_{GOx} from the stock solution in 1g L^{-1} BSA in PBS was added to the well plate and incubated for 1 h at RT while shaking at 100 rpm. After incubation, the plate was washed with 400 µL of PBS-Tween for 3 times to overcome unspecific binding followed by two additional rinsing steps with sodium citrate buffer (10 mM, pH 6.5) to remove PBS salt prior to the LSPR detection. Then, 200 µL of 400 mM glucose in 20 mM sodium citrate (pH 6.5) was added to each well and incubated for 1 h at 50 °C. Finally, 150 µL aliquots of each well after the enzymatic reaction were stored in 1.5 mL-amber vials (Thermo Fisher Scientific) equipped with 300 µL-polyspring insert (Thermo Fisher Scientific), which were nested to the multiposition valve of the flow system (see below) for automatic high-throughput hydrogen-peroxide mediated plasmonic NP detection.

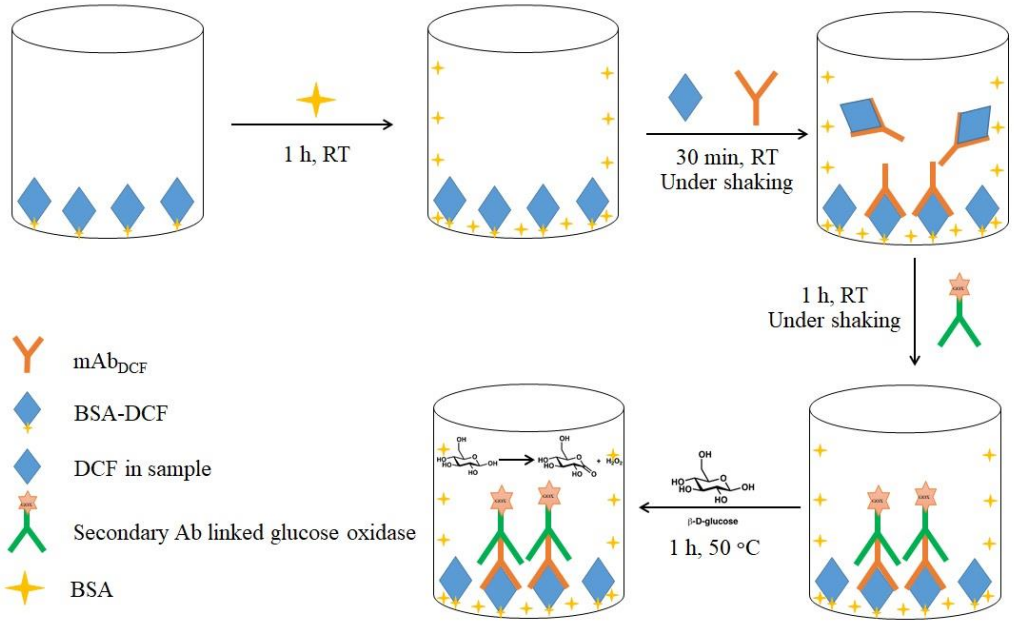

Figure 1 Schematic illustration of the microtiter plate-based competitive ELISA protocol for DCF prior to flow-through LSPR detection of AuNP

For comparison, a competitive microtiter plate ELISA for DCF was performed following the protocol described above but using an HRP-labelled secondary antibody (0.2 µg/mL in PBS; 200 µL/well) and colorimetric readout. After final washing, the substrate solution (200 µL/well) was added, and the plates were shaken for about 15 min for color development. Finally, the enzyme reaction was stopped with stop solution (100 µL/well) and the absorbance was read at 450 nm with a microplate reader (Synergy HT, Bio-Tek, Bad Friedrichshall, Germany). For construction of the calibration curves diclofenac standard solutions to cover the concentration range between 0.0001 to 100 µg L^{-1} were prepared in sea-salt (S9883, Merck, Germany) and also in tap water for comparison.

Fluidic setup for in-line LSPR detection using AuNP probes

The bespoke fluidic platform for in-line monitoring of the hydrogen-peroxide dependent generation of plasmonic AuNP is schematically illustrated in Fig. 2. It consists of (i) a 26-position low pressure stream selector C35Z-31826D (MPV) mounted on a microelectric actuator (VICI AG International, Schenkon, Switzerland), (ii) two bi-directional microsyringe pumps (SP, Cavro Xcalibur, Tecan Group Ltd, Männedorf, Switzerland) each furnished with

a 1-mL gas-tight glass syringe (Hamilton, Bonaduz, Switzerland) containing Milli-Q water (SP1) as a carrier, and 20 mM $HAuCl_4$ (SP2), respectively, and with a three-way head valve to either communicate with the flow system or aspirate reagent/carrier, (iii) a 10 mm path-length flow-through quartz cell (18 µL, Hellma GmbH, Müllheim, Germany), and (iv) a miniaturized USB4000 UV/VIS spectrometer (Ocean Optics, Largo, Florida, USA). The spectrometer is connected via a 300 µm optical fiber (QP300-1-SR-BX, Ocean Optics) to the ISS UV/VIS integrated sampling system (Ocean Optics) equipped with the light source and a direct attach cuvette holder. SP2 was covered by aluminum foil to prevent photochemical reactions of $HAuCl_4$. The flow manifold (including the holding coil, HC) was built from fluorinated ethylene propylene (FEP) tubing of 1/32" i.d. and 1/16" o.d., excepting the reaction coil that was made of perfluoroalkoxy alkane (PFA, 1/32" i.d. and 1/16" o.d.) with lengths shown in Fig. 2. The MPV was furnished with 10-32 nuts for connecting tubes, while other fluidic connections were made with ¼ 28" nuts with appropriate ferrules.

CocoSoft freeware[36] was selected as a user-friendly software for programming the motion and flow rates of the SP1 and SP2 and selection of the ports of the MPV throughout the flow method. SpectraSuite software (2008 Ocean Optic, 64-bit version 1.6.0.11) was used for control of the spectrometer detection parameters and data acquisition. Both software packages were synchronized for the sake of the unsupervised operation by CocoSoft proxying user's mouse clicks in pixels and times defined throughout the fluidic method as described below.

Automatic flow method for high-throughput DCF determination based on LSPR detection of AuNPs

After completion of the competitive ELISA for DCF in a well plate format, the resulting solution of the enzymatic reaction of glucose with GOx to yield hydrogen peroxide was transferred to the flow-based system by inserting the samples in Eppendorf tubes that were nested to ports 1 – 24 of the MPV, while the two remaining ports were used for aspiration of 1:5 (v/v) diluted aqua regia (as a rinsing solution of the flow manifold) and waste, respectively. The plasmonic gold nanoparticles were generated by in-line merging of 50 µL of hydrogen-peroxide and 20 mM citrate buffer containing sample solution (after aspiration from a given MPV port into the HC by SP1) with 50 µL of 0.6 mM $HAuCl_4$ in 0.5 mM HNO_3 from SP2 in a T-confluence by simultaneous activation of the two syringe pumps followed by pumping of the mixture toward the flow cell at 1.0 mL min^{-1} (see Fig. 2). The dispersed zone was then brought to the flow-through spectrophotometric cell to fill the

chamber volume (the remainder of the zone was kept in the PFA tubing) where it remained halted for a maximum of 10 min to yield plasmonic AuNPs. The LSPR spectra of AuNPs were recorded every 30 s with an integration time of 60 ms and a boxcar smoothing of 5 (11 pixels). The absorbance (A) was monitored continuously at 540 nm against a reference wavelength of 800 nm. To this end, virtual clicks from CocoSoft software opened the SpectraSuite window, clicked on the 'convert active spectrum to overlay' button, and minimized again the SpectraSuite program. This 3-click procedure was repeated every 30 s during the stopped-flow time of 10 min, thus accumulating a total number of 20 spectra that were recovered and processed anytime subsequently. After data acquisition, the nanoparticle-loaded plug was discarded, and the flow-through cuvette and tubing were flushed with 220 µL of 1:5 (v/v) diluted aqua regia at 1.0 mL min^{-1} by SP1 for dissolving potentially adsorbed nanoparticles and thus preventing fouling and cross contamination effects. The flow method ended by washing the reaction coil with 8000 µL of Milli-Q water at 1.0 mL min^{-1} from SP1. After automatic analysis of 24 samples, cleaning of the reaction coil with aqua regia overnight is recommended for removal of remnants of AuNP attached to the tubing walls. For every sample cohort analysis, the reaction time that allowed discrimination of blank against the EQS of DCF in seawater was adopted as an experimental parameter for samples and calibrants. The ratio of absorbance (A) for a given measurement against the maximum absorbance signal (A_0) of the LSPR peak obtained in the absence of DCF was selected as analytical readout ($Abs_{A/A0}$). A four parameter logistic sigmoidal regression of $Abs_{A/A0}$ against [DCF] was used as a standard calibration curve, yet linearization of the plot against log [DCF] within a predefined working range of concentrations was also investigated.

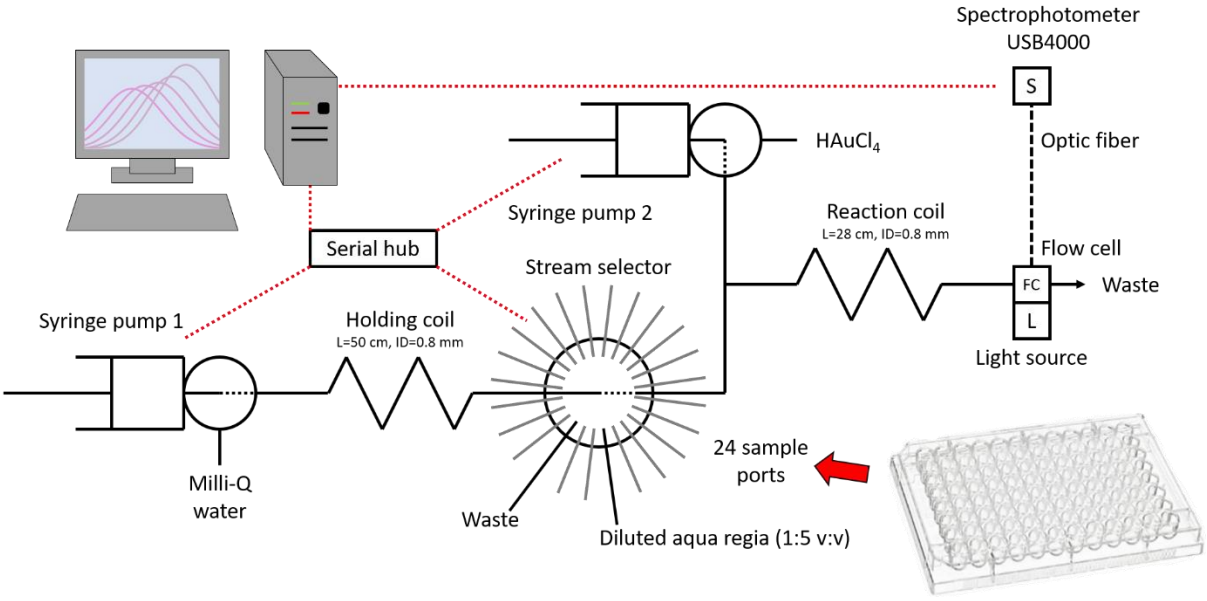

Figure 2 Schematic diagram of the automatic flow-through system for high-throughput ultrasensitive detection of DCF in seawater using plasmonic NP probes following competitive ELISA. SP (syringe pump), HC (holding coil), RC (reaction coil), FC (UV-Vis flow-through cell), D (detector).

RESULTS AND DISCUSSION

Investigation of experimental variables of the DCF competitive plasmonic immunoassay

Of the several experimental variables influencing the hydrogen peroxide yield of the competitive ELISA, both mAb_{DCF} and Ab_{GOx} are crucial factors for discrimination of blank versus ultratrace DCF concentrations on the basis of the maximum absorbance of the LSPR band (A_0 at 540 nm minus 800 nm) and the tonality change of the ensuing AuNPs across the flow system. Preliminary batchwise detection was accomplished by the addition of 100 µL of 0.5 mM Au(III) (pH= 6.8) after the mAb_{DCF}/Ab_{GOX}-based ELISA. The mAb_{DCF} concentration was investigated within the range spanning from 100 – 1,000 ng mL^{-1}, i.e., 1:50,000 to 1:5000 dilution under stagnant conditions for the plasmonic detection. The A_0 value along with the slopes obtained by linearization of the working range of the sigmoid curve (ca. 0.1-10 ng mL^{-1} DCF) increased with increasing the mAb_{DCF} concentration until 400 ng mL^{-1} (1:12,500 dilution) after which the surplus of mAb impaired the detection of ultratrace level concentration of DCF by the competitive ELISA and render poorer IC_{50} values (*viz.*, analyte concentration giving 50 % curve inhibition).[6] Likewise, a ca. 4-fold improvement of the slope of the linearized sigmoid curve and two-fold enhanced A_0 were observed by increasing the Ab_{GOx} concentration from 1:10,000 up to 1:1000 dilution, thus indicating the absence of

excess Ab_{GOx} under the experimental concentrations assayed. Therefore, the mAb_{DCF} and Ab_{GOx} dilutions from the stocks were set to 1:12,500 and 1:1000, respectively, for the remainder of the studies of the flow-through method.

The pH of the GOx catalyzed reaction after incubation with Ab_{GOx} is another yet critical parameter of the competitive ELISA, which will factor into the further development of the AuNPs and the particle size distribution thereof throughout the stopped-flow system (see next section). The pH range over which appropriate glucose turnover by GOx is reported in the literature[37,38] spans from 5.5 to 7.5, whilst Au(III) reduction by hydrogen peroxide with the subsequent NP nucleation necessitates pH values around 6.5 as indicated by Peng *et al.*[39] Hydrogen citrate/citrate buffer (pKa_3=6.4) was selected for pH adjustment to 6.5 with the additional advantage of using citrate as a co-reducing and stabilizing reagent of AuNPs in the flow system.[28,40,41] However, the concentration of the reducing buffer should be thoroughly investigated as a primary influent parameter on the morphology of AuNP. The absorbance of AuNPs at 540 nm increased with sodium citrate concentrations ranging from 2 mM up to 20 mM at a reaction time of 7 min, which most likely indicates faster nucleation rates, and, thus, smaller NP sizes would be generated. On the other hand, the increase of citrate concentration (investigated up to 30 mM) favored NP stabilization whereby excessively long reaction times might be called for across the flow system for appropriate method sensitivity against DCF. Therefore, a 20 mM hydrogen citrate/sodium citrate buffer (pH=6.5) was adopted for the enzymatic reaction and NP size control. The effect of glucose concentration and the enzymatic reaction time on the ELISA were also investigated from 50 – 800 mM and 15 – 90 min at 50 °C,[42] respectively. Glucose acts as the enzyme substrate but the surplus of the enzymatic oxidation might serve also as a co-reductant of Au(III)[43], thus ameliorating the AuNP nucleation kinetics. The higher the concentration of glucose (up to 400 mM) the higher was the slope of the linearized sigmoid curve. The enzymatic incubation time was fixed to 60 min inasmuch as the increase of H_2O_2 yield was proven negligible afterwards.

Investigation of critical parameters of the fluidic system for AuNPs nucleation and LSPR detection

Throughout the competitive ELISA, the lower the DCF concentration the higher the yield of H_2O_2 and thus the faster the nucleation and growth of NP is expected. As a consequence, smaller NP will be generated under flow conditions, and the hypsochromic (blue) shift of the LSPR band toward 540 nm is to be monitored unsupervised by the CocoSoft freeware.

Several flow configurations were initially investigated for the in-line formation of plasmonic NP under ultratrace concentrations of DCF (10-100 pg mL^{-1}). A simple one-line sequential injection system encompassing the sequential injection of 50 μL of solution from ELISA and 50 μL of Au(III) into the HC followed by pumping of the stacked zones by flow-reversal toward the flow-cell rendered poor sensitivity as a consequence of insufficient mutual penetration of the two plugs by axial dispersion in the way to the detection system. To surmount this problem, a hybrid fluidic configuration that in turn promotes radial mixing under laminar flow conditions was assembled instead by resorting to two simultaneously operating stand-alone microsyringe pumps (see Fig. 2). The flow rate toward the flow-through detector was affixed to 1.0 mL min^{-1} to assure a sufficient residence time to initiate nucleation across the reaction coil without excessive NP fouling onto the tubing walls.

The effect of critical parameters such as the Au(III) concentration and the tubing material of the reaction coil of the flow system on the plasmonic signals were studied in detail. Negatively charged tubing-solution interfaces are expected to offer enhanced nucleation rates of AuNP as signaled by Huang *et al.*[31] because the concentration of the initially positively charged citrate-Au(III) complexes generated in-line after the T-junction will increase locally on the reactor walls. The negatively charged citrate-capped nuclei will be repelled from the tubing and will be transferred along with the neutral gold seeds back into the bulk solution, thus facilitating optical monitoring of the kinetics of AuNP nucleation and growth while minimizing carryover effects of NP attached irreversibly on the manifold tubing. A variety of tubing materials of 0.8 mm i.d. with varying Z potential values at pH 6.5, *namely*, polyetheretherketone (PEEK), polytetrafluoroethylene (PTFE), fluorinated ethylene propylene (FEP) and perfluoroalkoxyalkane (PFA) were assayed. Experimental results demonstrated that the two tubing materials with the most negative surface potential at pH 6.5, i.e., PFA and FEP,[31] yielded smaller AuNPs with narrower size distribution at a given reaction time as identified by the high values of A_0 and narrow LSPR bands. The relative roughness of the four fluorinated tubing materials was also explored by scanning electronic microscopic (SEM) images and illustrated in Fig. S1. The SEM micrographs revealed that compared to PEEK and PTFE, PFA and FEP featured smoother inner surface, which is in good agreement with previous authors.[44,45] Based on our experimental findings, PFA was selected as the tubing material of the in-line reactor for efficient generation of smaller nanoparticle size and circumvent inter-assay AuNP fouling onto the inner surfaces by in-line rinsing with diluted aqua regia.[31]

The effect of Au(III) concentration and the Au(III)/citrate ratio on the sensitivity of the flow-through plasmonic method and the dynamic range for DCF was investigated within the range of 0.3 – 0.7 mM Au(III) by in-line merging of the gold solution with the hydrogen peroxide containing sample obtained by calibration of the ELISA with distinct concentrations of DCF. The higher the Au(III) concentration (up to 0.6 mM) the smaller the relative nanoparticle size and the larger difference of Abs_A at 540 nm were obtained for 10 pg mL^{-1} against 10 ng mL^{-1} DCF (see Fig. S2). The reagent concentration was affixed to 0.6 mM Au(III) that rendered a final citrate to gold molar ratio of ca. 33 and a final concentration of Au(III) of 0.3 mM throughout the flow-through PFA reactor.

Under the aforementioned experimental physicochemical conditions of the flow method, the nucleation rates of plasmonic AuNP were monitored over time (up to 10 min) in a fully automatic mode (see spectra in Fig. S3). The LSPR spectra obtained on-line at varied DCF concentrations at a fixed reading time of 5.5 min are illustrated in Fig. S4. The difference between the LSPR absorbance at the maximum wavelength (λ_{max}=540 nm) and reference wavelength (λ_{ref}=800 nm) was used as analytical readout to generate the signal-time curves at increasing concentrations of DCF as shown in Fig. 3. The suitable time window of AuNPs nucleation and growth for discrimination and quantification of 10 pg mL^{-1} DCF in seawater against lower concentrations of DCF (1 pg mL^{-1} and below) corresponds to 4 – 7 min (see Fig. 3). By processing of the recorded LSPR spectra throughout the automatic system, the best reaction time for plotting of the calibration graph and undertake the ultrasensitive determination of DCF in seawater can be readily tuned intra- and inter-day unsupervised.

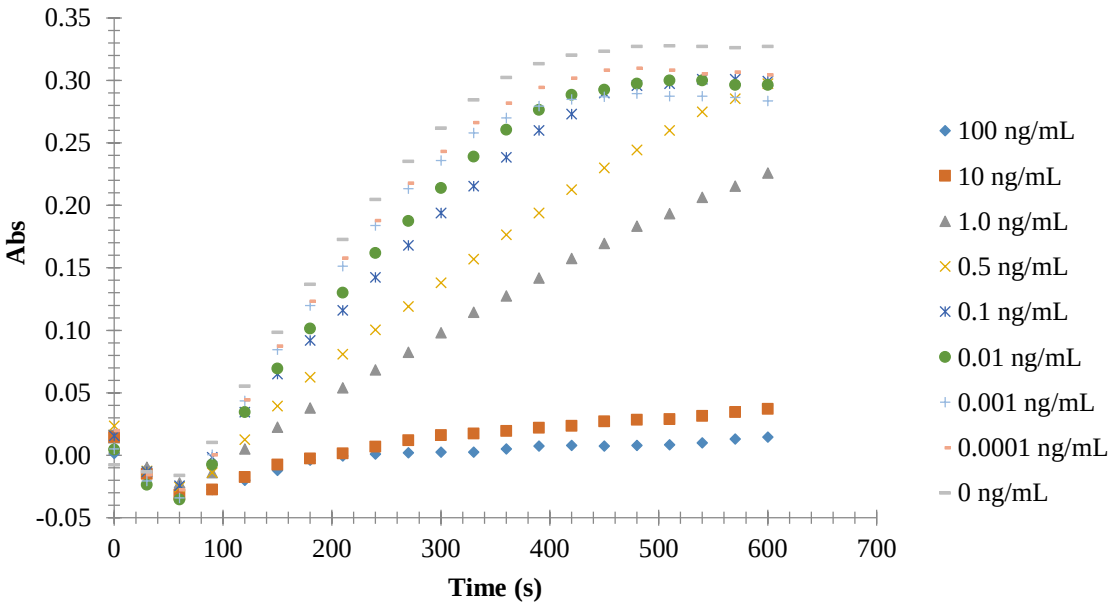

Figure 3. Monitoring of the in-line generation of hydrogen-peroxide mediated AuNP over time at varied DCF concentrations by resorting to the stopped-flow fluidic platform. Absorbance data are given as readouts at 540 nm (analytical wavelength) minus 800 nm (reference wavelength) up to 10 min

Analytical performance of the flow system and real sample analysis

The analytical performance of the automatic flow-through LSPR absorbance method for ultratrace determination of DCF was studied in terms of dynamic range, sensitivity, intermediate precision, limits of detection and quantification, and application of real seawater samples. A 4-parameter logistic sigmoid curve of Abs(A/A_0) against DCF concentration was plotted within the range of 0-100 ng mL^{-1} DCF using DCF-free seawater (as identified by HPLC-MS following solid-phase extraction) for matrix-matched calibration. The sigmoid standard curve (see Fig. 4) was fitted to:

$$\mathrm{Abs}\left(\frac{\mathrm{A}}{\mathrm{Ao}}\right) = 0.044 + \frac{0.982}{1+\left(\frac{[\mathrm{DCF}\left(\frac{\mathrm{ng}}{\mathrm{mL}}\right)]}{0.792}\right)^{0.710}}$$

with a correlation coefficient of 0.9942, yet a dynamic linear range over three-decade log scale, *namely*, 0.01 – 10 µg L^{-1} DCF using the equation (Abs(A/A_0) = -0.27×log [DCF (ng mL^{-1})] + 0.34 (R^2=0.9984) could be harnessed instead for the sake of rapid quantification of DCF (see inset in Fig. 4). The linear range equates to a concentration range of 50-400 µM hydrogen peroxide as determined by external calibration with standard solutions of hydrogen peroxide. The limits of detection (LOD) and quantitation (LOQ) based on the $3s_b$ and $10s_b$ criteria (n=7) were calculated from the normalized calibration as the concentrations equating to 1-$3s_b$ and 1-$10s_b$, respectively, which corresponded to 0.001 and 0.003 µg L^{-1} DCF, respectively. For the sake of comparison, the analytical performances of the batchwise plasmonic ELISA and the conventional colorimetric ELISA have been also investigated. A linear range of 0.1-100 µg L^{-1} and 0.03-0.16 µg L^{-1} DCF along with an LOD of 0.08 µg L^{-1} DCF and 0.018 µg L^{-1} DCF have been obtained for the plasmonic and the colorimetric ELISA, respectively (see Figs S5 and S6). It should be noted that the LOD of the batchwise ELISA counterpart is one order of magnitude above the maximum acceptable method detection limit specified by the EU Commission for DCF in seawater (viz., 0.01 µg L^{-1} DCF). The LOD of the colorimetric ELISA is much closer to the critical value but the required detectability could not be reached as well. Further, the LOD and dynamic range of the flow-through SPR system are on a par with those reported in the literature for determination of DCF in seawater by HPLC/UHPLC-MS[46-48] but with no need of prior solid-phase

preconcentration and matrix clean-up/desalting protocols (see Table S1 for details), and at least one order of magnitude better than most of the previous ELISA, immunosensors or cell sensors for diclofenac,[6,49,50,51,52,53], which to the best of our knowledge have been merely applied to freshwaters and industrial waters but saline or hypersaline waters (see Table S2). This is most likely a consequence of high matrix interfering effects of saline matrices in the detection scheme that can be overcome by using the flow-based kinetic-controlled detection system herein reported. It should be also stressed the fact that the reproducibility of manual immunoassays/biosensors might amount to RSD values as high as 23-100%.[6,49,50,54] Most importantly, the minimum spiked concentration level of DCF in all of the previous works spanned from 15-1000 ng/L,[6,49-52,54-56] again indicating that none of the immunoassays is suitable for determination of DCF at the environmental quality standard level set in seawater, that is, 10 ng/L.

The precision of the proposed fluidic method was studied at three distinct concentration levels of DCF in seawater that covered three orders of magnitude, viz., 0.01, 0.1 and 1.0 ng mL^{-1}. The intra-day relative standard deviations (%RSD of normalized signal readouts, n = 5) at a reaction time of 7 min were 1.4%, 3.0% and 3.2%, respectively, thus indicating a good repeatability in AuNP nucleation and growth under flow regime. The inter-day intermediate precision values at 0.01, 0.1, and 1.0 ng mL^{-1} levels in seawater increased up to 3.9, 13.6 and 10.8%, respectively, but were significantly better than those obtained with the batchwise counterpart with RSD values of 16.0, 14.3, and 30.0%, respectively.

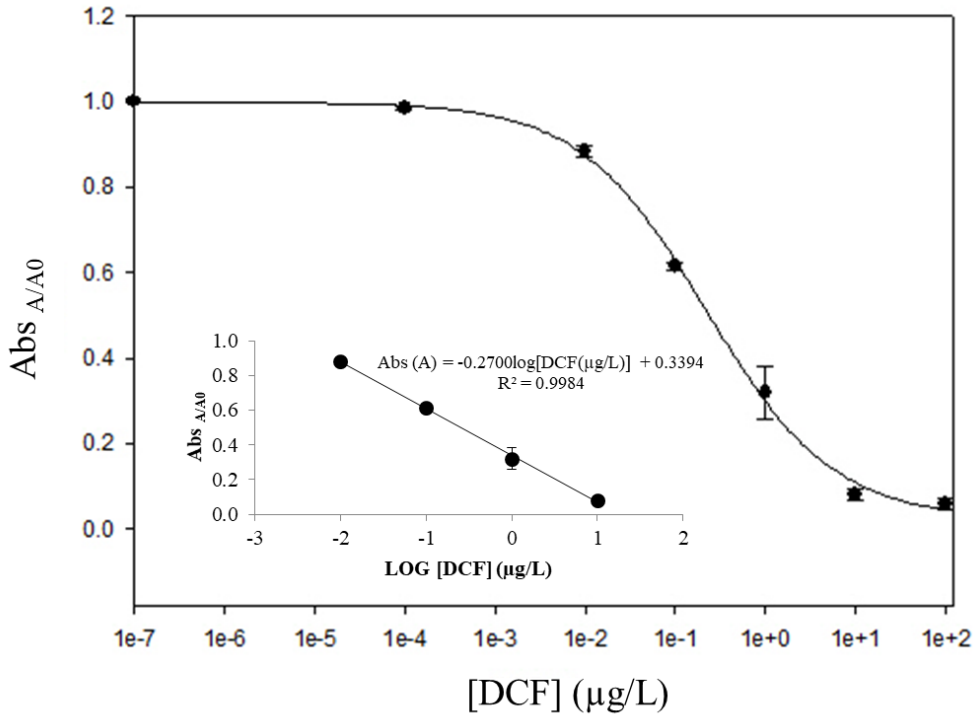

Figure 4. Logistic sigmoid calibration curve of LSPR absorbance of AuNP as obtained by the flow-through platform following the competitive ELISA under matrix matched conditions. The inset illustrates the dynamic linear range from 0.01 up to 10 µg L^{-1} DCF at a stopped flow time of 7 min. Error bars are given as standard deviation (n=3)

The trueness (lack of bias) of the flow-through AuNP-based LSPR method was ascertained by direct analysis of spiked coastal seawater sampled at various beaches in Mallorca island (see Experimental) using the linear calibration curve. None of the real samples contained detectable DCF, *viz.*, [DCF] < 2 ng L^{-1}, as determined by solid phase extraction using Oasis HLB followed by reversed-phase (C18)-HPLC-MS detection according to the protocol by Huebner *et al.*[6] Every sample was spiked at two distinct concentration levels, viz., 0.01 ng mL^{-1} and 0.1 ng mL^{-1} DCF, the former being the maximum allowed concentration of DCF in seawater endorsed by the EU Watch List. The relative recoveries ranged in all instances from 90-106% (see Table 1), thus indicating the absence of multiplicative matrix interferences throughout the ELISA and the flow-through LSPR sensing method, making the use of the method of the standard additions unnecessary.

Table 1. Relative recoveries of DCF in seawater samples as determined by ELISA in combination with on-line LSPR absorbance detection of AuNP

Sample	Added (ng mL^{-1})	Found (µg L^{-1})	Recovery (%)
S'Estanyol	0.01	0.009±0.001	90±10
	0.1	0.094±0.005	94±5
Port de Pollensa	0.01	0.010±0.001	100±10
	0.1	0.099±0.003	99±3
Santa Ponsa (Winter)	0.01	0.0102±0.0009	102±9
	0.1	0.099±0.010	99±10
Santa Ponsa (Spring)	0.01	0.0106±0.0003	106±3
	0.1	0.103±0.002	103±2

CONCLUSION

A bespoke flow-through system is herein proposed for the first time as a reliable platform for automatic monitoring of the nucleation and growth rates of AuNPs. The plasmonic NP are used as nanoprobes for high-throughput LSPR determination of diclofenac, which is taken as a model of an environmental emerging contaminant. The flow manifold was built for unsupervised analysis of up to 24 samples containing varying levels of hydrogen peroxide from competitive ELISA. By using user-friendly software for programming of hydrodynamic variables and data recording, the proposed (meso)fluidic platform features (i) automatic injection of microliter volumes of sample and Au(III), (ii) controllable mixing of solutions and in-line generation of AuNP, and (iii) unsupervised recording of time-resolved LSPR absorption bands, thus overcoming the reported limitations of batchwise plasmonic ELISA for reliable quantitative analysis. Without any prior sample processing method, our fluidic approach is capable of determining diclofenac in troublesome samples (e.g., seawater) at concentrations down to 10 ng L^{-1}, that is, below those endorsed by the EU Watch List for potential emerging contaminants and the conventional colorimetric ELISA.

Current research work is underway in our lab to expand the scope of applicability of the fluidic LSPR absorbance platform to ultratrace determination of other emerging organic

contaminants listed by the Watch List in combination with mAb-based highly sensitive ELISA using enzymes other than oxidases.

Supporting information: Detailed description and information of (i) reagent and solutions; (ii) morphology of the inner walls of the flow-through reactor; (iii) effect of the Au(III) concentration on the size of the plasmonic gold nanoparticles and LSPR absorption bands; and (iv) time-resolved LSPR absorption spectra and influence of DCF concentration.

Acknowledgments

Manuel Miró, Miquel Oliver and David J. Cocovi-Solberg acknowledge financial support from the Spanish Ministry of Science, Innovation and Universities (MCIU) and the Spanish State Research Agency (AEI) through projects CTM2017-84763-C3-3-R (MCIU/AEI/FEDER, EU) and CTM2017-90890-REDT (MCIU/AEI/FEDER, EU). Technical assistance by Dr. de la Rica is greatly appreciated. The Thailand Research Fund (TRF), the Commission on Higher Education, Faculty of Science, and Chiang Mai University are acknowledged for funding support. The Royal Golden Jubilee (RGJ) Ph.D. Program is gratefully acknowledged for the scholarship to N. Kaewwonglom (NK). NK also thanks the FI-TRACE group at the University of Balearic Islands for scientific supervision and availability of instrumentation, and the Graduate School of Chiang Mai University for financial support.

REFERENCES

(1) Drijvers, J. M.; Awan, I. M.; Perugino, C. A.; Rosenberg, I. M; Pillai, S. The Enzyme-Linked Immunosorbent Assay: The Application of ELISA in Clinical Research, In Jalali, M.; Saldanha, F. Y. L.; Jalali, M., Eds.; Basic Science Methods for Clinical Researchers, Academic Press:Boston, 2017; ch.7, pp.119-133.

(2) Krall, A. L.; Elliott, S. M.; Erickson, M. L.; Adams, B. A. Detecting sulfamethoxazole and carbamazepine in groundwater: Is ELISA a reliable screening tool? *Environ. Pollut.* **2018**, *234*, 420-428.

(3) Zhu, N.-F.; Zhu, Y.-Q.; Wang, J.; Gyimah, E.; Hu, X.-L.; Zhang, Z. A novel fluorescence immunoassay based on AgNCs and ALP for ultrasensitive detection of sulfamethazine (SMZ) in environmental and biological samples. *Talanta* **2019**, *199*, 72-79.

(4) González-Martínez, M. Á.; Puchades, R.; Maquieira, Á. Immunoanalytical Technique: Enzyme-Linked Immunosorbent Assay (ELISA), In Sun, D-W., Ed.; Modern Techniques for Food Authentication, 2nd Ed., Academic Press: Boston, 2018, ch.15, pp. 617-657.

(5) Zhang, Z.; Zeng, K.; Liu, J.-F. Immunochemical detection of emerging organic contaminants in environmental waters.*TrAC-Trends Anal.Chem.* **2017**, *87*,49-57.

(6) Huebner, M.; Weber, E.; Niessner, R.; Boujday, S.; Knopp, D. Rapid analysis of diclofenac in freshwater and wastewater by a monoclonal antibody-based highly sensitive ELISA. *Anal. Bioanal. Chem.* **2015**, *407*, 8873-8882.

(7) Sogawa, R.; Saita, T.; Yamamoto, Y.; Kimura, S.; Narisawa, Y.; Kimura, S.; Shin, M. Development of a competitive enzyme-linked immunosorbent assay for therapeutic drug monitoring of afatinib. *J. Pharm. Anal.* **2019**, *9*, 49-54.

(8) Sanchis, A.; Bosch-Orea, C.; Salvador, J.P.; Marco,M. P.; Farré, M. Development and validation of a multianalyte immunoassay for the quantification of environmental pollutants in seawater samples from the Catalonia coastal area. Anal. Bional. Chem. **2019**, in the press. DOI: 10.1007/s00216-019-01971-3.

(9) Antunes, J.; Justino, C.; Pinto da Costa, J.; Cardoso, S.; Duarte, A.C.; Rocha-Santos, T. Graphene immunosensors for okadaic acid detection in seawater. *Microchem. J*. **2018**, *138*, 465–471.

(10) Liang, Y.; Huang, X.-L.; Chen, X.-R.; Zhang, W.-J.; Ping, G.; Xiong, Y.-H. Plasmonic ELISA for naked-eye detection of ochratoxin A based on the tyramine-H_2O_2 amplification system. *Sens. Actuators, B:Chem.* **2018**, *259*, 162-169.

(11) Xiong, Y.; Pei, K.; Wu, Y.-Q.; Duan, H.; Lai, W.-H.; Xiong,Y.-H. Plasmonic ELISA based on enzyme-assisted etching of Au nanorods for the highly sensitive detection of aflatoxin B1 in corn samples. *Sens. Actuators,B:Chem*. **2018**, *267*, 320-327.

(12) Ma, X.-M.; Chen, Z-T.; Kannan, P.; Lin, Z.-Y.; Qiu, B.; Guo, L-H. Gold nanorods as colorful chromogenic substrates for semiquantitative detection of nucleic acids, proteins, and small molecules with the naked eye. *Anal.Chem.* **2016**, *88*, 3227-3234.

(13) de la Rica, R.; Stevens, M. M. Plasmonic ELISA for the detection of analytes at ultralow concentrations with the naked eye. *Nature Prot.* **2013**, *8*, 1759-1764.

(14) Zhang, Z.-Y.; Wang, H.; Chen, Z.-P.; Wang, X.-Y.; Choo, J.; Chen, L.-X. Plasmonic colorimetric sensors based on etching and growth of noble metal nanoparticles: Strategies and applications. *Biosens. Bioelectron.* **2018**, *14*, 52-65.

(15) Zhang, Y.-L.; McKelvie, I. D.; Cattrall, R. W.; Kolev, S. D. Colorimetric detection based on localised surface plasmon resonance of gold nanoparticles: Merits, inherent shortcomings and future prospects. *Talanta* **2016**, *152*, 410-422.

(16) Liang, J.-J.; Yao, C.-Z.; Li, X.-Q.; Wu, Z.; Huang, C.-H.; Fu, Q.-Q.; Lan, C.-F.; Cao, D.-L.; Tang, Y. Silver nanoprism etching-based plasmonic ELISA for the high sensitive detection of prostate-specific antigen. *Biosens. Bioelectron.* **2015**, *69*, 128-134.

(17) Lin,Y.; Xu, S.-H.; Yang, J.; Huang, Y.-J.; Chen, Z.-T.; Qiu, B.; Lin, Z.-Y.; Chen, G.-N.; Guo, L.-H. Interesting optical variations of the etching of Au Nanobipyramid@Ag Nanorods and its application as a colorful chromogenic substrate for immunoassays. *Sens. Actuators, B:Chem.* **2018**, *267*, 502-509.

(18) Zhan, L.; Wu, W. B.; Yang, L.; Huang, C. Z. Sensitive detection of respiratory syncytial virus based on a dual signal amplified plasmonic enzyme-linked immunosorbent assay. *Anal. Chim. Acta* **2017**, *962*, 73-79.

(19) Cecchin, D.; de la Rica, R.; Bain, R. E. S.; Finnis, M. W.; Stevens, M. M.; Battaglia, G. Plasmonic ELISA for the detection of gp120 at ultralow concentrations with the naked eye. *Nanoscale* **2014**, *6*, 9559-9562.

(20) De la Rica; R.; Stevens, M. M. Plasmonic ELISA for the ultrasensitive detection of disease biomarkers with the naked eye. *Nat. Nanotechnol.* **2012**, *7*, 821-824.

(21) Gobbo, P.; Biondi, M. J.; Feld, J. J.; Workentin, M. S. Arresting the time-dependent H_2O_2 mediated synthesis of gold nanoparticles for analytical detection and preparative chemistry. *J. Mater. Chem. B* **2013**, *1*, 4048-4051.

(22) Wang, X.; Niessner, R.; Knopp, D. Controlled growth of immunogold for amplified optical detection of aflatoxin B1. *Analyst* **2015**, *140*, 1453-1458.

(23) Pubpeer publications, https://pubpeer.com/publications/54AECF24E96162E3A563AED08BE0B3 (last accessed date 21st August 2019)

(24) Lévy, R. Homeopathic Nanoparticles, In Three Little (Nano)Controversies and Their Morals; available at https://raphazlab.wordpress.com/2017/09/20/three-little-nano-controversies-and-their-morals (last accessed date 21st August 2019).

(25) Miró, M.; Hansen, E. H. Miniaturization of environmental chemical assays in flowing systems:The lab-on-a-valve approach vis-à-vis lab-on-a-chip microfluidic devices. *Anal. Chim. Acta* **2007**, *600*, 46-57.

(26) Passos, M. L. C.; Pinto, P. C. A. G.; Santos, J. L. M.; Saraiva, M. L. M. F. S.; Araujo, A. R. T. S. Nanoparticle-based assays in automated flow systems: A review. *Anal. Chim. Acta* **2015**, 889, *22*-34.

(27) Passos, M. L. C.; Costa, D.; Lima, J. L. F. C.; Saraiva, M. L. M. F. S. Sequential injection technique as a tool for the automatic synthesis of silver nanoparticles in a greener way. *Talanta* **2015**, *133*, 45-51.

(28) Baber, M. R. *Synthesis of inorganic nanoparticles using microfluidic devices*, PhD Thesis, University College London:UK, 2017.

(29) Ftouni, J.; Girardon, J. S.; Penhoat, M.; Payen, E.; Rolando, C. Gold nanoparticle synthesis in microfluidic systems and immobilisation in microreactors designed for the catalysis of fine organic reactions. *Microsyst.Technol.* **2012**, *18*, 151-158.

(30) Hao, N.; Nie, Y.; Zhang, J. X. J. Microfluidic synthesis of functional inorganic micro-/nanoparticles and applications in biomedical engineering. *Int. Mater. Rev.* **2018**, *63*, 461-487.

(31) Huang, H.; Toit, H. D; Besenhard, M. O.; Ben-Jaber, S.; Dobson, P.; Parkin, I.; Gavriilidis, A. Continuous flow synthesis of ultrasmall gold nanoparticles in a microreactor using trisodium citrate and their SERS performance. *Chem. Eng. Sci*. **2018**, *189*, 422-430.

(32) Trojanowicz, M. Flow chemistry vs. flow analysis. *Talanta* **2016**, *46*, 621-640.

(33) Bonnefille, B.; Gomez, E.; Courant, F.; Escande, A.; Fenet, H. Diclofenac in the marine environment: A review of its occurrence and effects. *Mar. Pollut. Bull.* **2018**, *131*, 496-506.

(34) Lonappan, L.; Brar, S. K.; Das, R. K.; Verma, M.; Surampalli, R. Y. Diclofenac and its transformation products: Environmental occurrence and toxicity - A review. *Environ .Int.* **2016**, *96*, 127-138.

(35) Commission Implementing Decision (EU) 2015/495 of 20 March 2015 establishing a watch list of substances for Union-wide monitoring in the field of water policy pursuant to Directive 2008/105/EC of the European Parliament and of the Council. *Off. J. Eur. L* **2015**, *78*, 40-42.

(36) Cocovi-Solberg, D.J.; Miró, M. CocoSoft: Educational software for automation in the analytical chemistry laboratory. *Anal. Bioanal. Chem.* **2015**, *407*, 6227-6233.

(37) Bankar, S. B.; Bule, M. V.; Singhal, R. S.; Ananthanarayan, L. Glucose oxidase — An overview, *Biotechn. Adv.* **2009**, *27*, 489-501.

(38) Odebunmi, E.; Owalude, S. Kinetic and thermodynamic studies of glucose oxidase catalysed oxidation reaction of glucose. *J. Appl. Sci. Environ. Manage.* **2007**, *11*, 95-100.

(39) Peng, C.-F.; Dan, X.-H.; Xie, Z.-J.; Liu, C.-L. Shape-controlled generation of gold nanoparticles assisted by dual-molecules: The development of hydrogen peroxide and oxidase-based biosensors. *J. Nanomater.* **2014**, 576082.

(40) Giri, B. Synthesis of gold nanoparticles on microchip, In Giri, B. Ed.; Laboratory Methods in Microfluidics, Elsevier:The Netherlands, 2017, ch. 16, pp.103-107.

(41) Ji, X.-H.; Song, X.-N.; Li, J.; Bai, Y.-B.; Yang, W.-S.; Peng, X.-G. Size control of gold nanocrystals in citrate reduction: The third role of citrate. *J. Am. Chem. Soc.* **2007**, *129*, 13939-13948.

(42) Yang, Y.-C.; Tseng, W.-L. 1,4-Benzenediboronic-acid-induced aggregation of gold nanoparticles: Application to hydrogen peroxide detection and biotin–avidin-mediated immunoassay with naked-eye detection. *Anal. Chem.* **2016**, *88*, 5355-5362.

(43) Liu, J.-C.; Qin, G.-W.; Raveendran, P.; Ikushima, Y. Facile "Green" Synthesis, Characterization, and Catalytic Function of β-D-Glucose-Stabilized Au Nanocrystals. *Chem. Eur. J.* **2006**, *12*, 2131-2138.

(44) McKeen, L. W. High-temperature and high-performance polymers, In McKeen, L. W.,Ed.; Permeability Properties of Plastics and Elastomers, 3rd Ed., William Andrew Publishing:Oxford, 2012, ch.11, pp. 233-250.

(45) Hecht, K. Microreactors for gas/liquid reactions: The role of surface properties, PhD Dissertation, Karlsruhe Institute of Technology, Germany, 2013.

(46) Wu, J.-M.; Qian, X.-Q.; Yang, Z.-G.; Zhang, L.F. Study on the matrix effect in the determination of selected pharmaceutical residues in seawater by solid-phase extraction and ultra-high-performance liquid chromatography–electrospray ionization low-energy collision-induced dissociation tandem mass spectrometry. *J. Chromatogr. A* **2010**, *1217*, 1471-1475.

(47) Magnér, J.; Filipovic, M.; Alsberg, T. Application of a novel solid-phase-extraction sampler and ultra-performance liquid chromatography quadrupole-time-of-flight mass spectrometry for determination of pharmaceutical residues in surface sea water. *Chemosphere* **2010**, *80*, 1255-1260.

(48) Pereira, C. D. S.; Maranho, L. A.; Cortez, F. S.; Pusceddu, F. H.; Santos, A. R.; Ribeiro, D. A.; Cesar, A.; Guimarães, L. L. Occurrence of pharmaceuticals and cocaine in a Brazilian coastal zone. *Sci. Total Environ.* **2016**, *548-549*, 148-154.

(49) Hlaváček, A.; Peterek, M.; Farka, Z.; Mickert, M.J.; Prechtl, L.; Knopp, D.; Gorris, H.H. Rapid single-step upconversion-linked immunosorbent assay for diclofenac. *Microchim. Acta* **2017**, *184*, 4159–4165.

(50) Hlaváček, A.; Farka, Z.; Hübner, M.; Horňáková, V.; Němeček, D.; Niessner, R.; Skládal, P.; Knopp, D.; Gorris, H.H. Competitive upconversion-linked immunosorbent assay for the sensitive detection of diclofenac. *Anal. Chem.* **2016**, *88*, 6011-6017.

(51) Steinke, N.; Döring, S.; Wuchrer, R.; Kroh, C.; Gerlach, G.; Härtling, T. Plasmonic sensor for on-site detection of diclofenac molecules. *Sens. Actuators, B: Chem.* **2019**, *288*, 594-600.

(52) Shi, J.; Xu, M.-X.; Tang, Q.-H.; Zhao, K.; Deng, A.; Li., J.-G. Highly sensitive determination of diclofenac based on resin beads and a novel polyclonal antibody by using flow injection chemiluminescence competitive immunoassay. *Spectrochim. Acta, A* **2018**, *191*, 1-7.

(53) Schirmer, C.; Posseckardt, J.; Schroder,M.; Glaser,M.; Howitz,S.; Scharff,W.; Mertig, M. Portable and low-cost biosensor towards on-site detection of diclofenac in wastewater. *Talanta* **2019**, *203*, 242-247.

(54) Nguyen, T. T. K.; Vu, T. T.; Anquetin, G.; Tran, H. V.; Reisberg, S.; Noël, V.; Mattana, G.; Nguyen, Q. V.; Lam, T. D.; Pham, M. C.; Piro, B. Enzyme-less electrochemical displacement heterogeneous immunosensor for diclofenac detection. *Biosens. Bioelectron.* **2017**, *97*, 246-252.

(55) Wang, C.; Jiang,T.-X.; Zhao, K.; Deng, A.; Li., J.-G. A novel electrochemiluminescent immunoassay for diclofenac using conductive polymer functionalized graphene oxide as labels and gold nanorods as signal enhancers. *Talanta* **2019**, *193*, 184-191.

(56) Hu, L.-Y.; Zheng, J.; Zhao, K.; Deng, A.; Li., J.-G. An ultrasensitive electrochemiluminescent immunosensor based on graphene oxide coupled graphite-like carbon nitride and multiwalled carbon nanotubes-gold for the detection of diclofenac. *Biosens. Bioelectron.* **2018**, *101*, 260-267.

TOC